IEEE Access
Multidisciplinary | Rapid Review | Open Access Journal

Received April 7, 2020, accepted April 26, 2020, date of publication May 6, 2020, date of current version May 19, 2020.

Digital Object Identifier 10.1109/ACCESS.2020.2992558

DC-DC Linearized Converter Model for Faster Simulation of Lightweight Urban Electric Vehicles

FRANCISCO J. GÓMEZ NAVARRO[1], LUIS J. YEBRA[2], FRANCISCO J. GÓMEZ MEDINA[3], AND ANTONIO GIMÉNEZ-FERNANDEZ[1]

[1]Centro Mixto CIESOL, Universidad de Almería, 04120 Almería, Spain
[2]CIEMAT, Plataforma Solar de Almería, 04200 Almería, Spain
[3]Department of Engineering, Institute for Manufacturing, University of Cambridge, Cambridge CB3 0FS, U.K.

Corresponding author: Francisco J. Gómez Navarro (fgn891@inlumine.ual.es)

This work was supported in part by the Spanish Ministry of Economy, Industry, and Competitiveness (National R + D + i Plan Project) under Grant DPI2017-85007-R, and in part by the European Regional Development Fund (ERDF).

ABSTRACT The aim of this paper is to present a new bidirectional DC-DC linearized converter model for use in power demand and recovery units mainly used in Lightweight Electric Vehicle applications. The model significantly reduces the simulation time of the experiments performed, with up to a 4450-fold decrease in simulation times with respect to the original switched DC-DC topology. The study begins with a literature review of available switched converters, after which the presented topology is selected. The object-oriented modeling language Modelica® is used to implement the converter in the Dymola® modeling environment. Components and base classes from the Modelica Standard Library and VehicleInterfaces library are mainly used for better interoperability. Because of the intensive use of converters in the whole vehicle and the time consumed by the converter simulations due to high frequency commutation, a linearized DC-DC converter model is proposed. Comparison tests are performed between the reference switched models and the proposed linearized models in Dymola® tool to validate the linearized model behaviour. Nearly identical responses are obtained for both models, while simulation times are reduced as much as 1/4450 for the linearized converter. Furthermore, validation tests are carried out between the proposed linearized model in Dymola® and a reference switched model in LTspice® specific purpose simulation package for switched electronic circuits. Excellent agreement in the responses of both models is observed.

INDEX TERMS Computer simulation, continuous time systems, discrete-time systems, DC-DC power converters, energy efficiency, energy management, smart grids.

I. INTRODUCTION

The Intergovernmental Panel on Climate Change (IPCC) states that CO_2 global emissions must be halved by 2050 with respect to 2000 levels, by which time as much as 80% of the total energy consumption is expected to result from transport alone [1], [2]. The European Commission has also established the foundations for the creation of competitive and sustainable transport policies, among which stand out the progressive reduction of Internal Combustion vehicles in urban settings and encouraging the use of smaller, lighter passenger vehicles specifically designed for urban transport [3].

A Smart Energy Hub (SEH) [4] comprising all elements of the Electric Vehicle (EV) that generate or consume energy would enable dynamic simulation of the full vehicle, as well as evaluation and optimization of control algorithms and smart energy management systems, once suitable models have been created for each of the elements comprising the SEH. This would ultimately allow analysis of energy flows and vehicle behaviour under various scenarios and configurations. Simulation results could also be contrasted with those of other authors. The concept of SEH is based on a decentralized architecture of the vehicle's electrical system, where each electrical subsystem connects to an intermediate DC-link. Each electrical subsystem acts as a standalone unit, which connects to the DC-Link via either an input converter, an output converter, or both. The advantages of this configuration are discussed in more detail in [5]. Given the role of converters to adjust the power flow demands of each subsystem, these play a key role in vehicle behaviour and management of energy demands. Therefore, the dynamic models of these converters must be reliable and allow for reasonable simulation timeframes.

The associate editor coordinating the review of this manuscript and approving it for publication was Huazhu Fu.

This paper focuses on Pulse Width Modulation (PWM) DC-DC converters, which have been extensively employed over the last few decades in applications where a wide spectrum of output power is needed. These converters are particularly advantageous due to their low number of components, high efficiency, fixed frequency operation, relatively simple control and high voltage conversion ratios in buck and boost modes. Their main disadvantage lies in losses associated with commutation, which limit the maximum frequency at which the converter can be operated. Reference [6] describes the most common PWM DC-DC converter configurations and presents their respective characteristic equations which can be used for component specification and dimensioning. Of particular significance are the basic converter (non-isolated buck/boost converter) and flyback converter (isolated buck/boost converter, in mono and bidirectional modes). The use of converters with two independent switches is shown in [7] to reduce stress in its components relative to its single-switch counterpart, irrespective of it being buck, boost or buck/boost. Two different bidirectional converter configurations are compared in [8] (bidirectional buck/boost and cascaded bidirectional buck/boost converter); this study concluded that the cascaded topology exerts lower thermal and electric stresses on its components, and despite the higher number of components, the smaller solenoid and capacitor dimensions required constitute an acceptable trade-off. The non-isolated cascaded bidirectional buck/boost converter topology is proposed in works such as [9], who presents a non-isolated bidirectional buck/boost converter with three commutators and cascaded connection for energy management of batteries in uninterrupted energy supply systems. Reference [10] proposes a synchronous unidirectional buck/boost converter for battery management systems in solar photovoltaic installations, [11] proposes a four-quadrant bidirectional buck/boost converter for use in EVs, [12] proposes a unidirectional buck/boost converter for use in fuel-cell EVs, and [13] presents a similar configuration, albeit unidirectional, for its use as a Maximum Power Point Tracking System in a photovoltaic solar plant. A comparison of several non-isolated bidirectional DC-DC converter configurations for their use in Hybrid Electric Vehicles is presented in [14]. In this work, we proposed a simplified version of a cascaded buck/boost converter termed Half-Bridge converter, which possesses all the advantages of a cascaded converter whilst also being comprised of a lower number of components; this converter is best suited for applications where it is not necessary to switch between buck and boost modes for a particular flow direction. This converter topology is used in [15] and [16] for similar applications.

The converters in the battery and motor have a significant impact on vehicle performance, since these components experience the largest energy flows of the SEH. The battery and motor can act both as sinks and sources of energy depending on the vehicle operating conditions, and hence these converters must be bi-directional. Highly reliable models have been produced in recent literature for battery behaviour [17]. However, the battery behaviour itself is non-linear and battery voltage varies with electrical load. Therefore, the motor converter is the focus of this work.

This work proposes a Non-isolated Bidirectional Half-Bridge DC-DC Converter (NBHBC) model for energy delivery during powering of the motor and energy harvesting during braking. Nominal voltages are defined as 48Vdc for the SEH and 36 Vdc for the motor. This voltage specification allows for simplification of the converter, which operates in buck mode when the motor consumes energy and boost mode during regenerative braking. The DC-DC converters mentioned above are switched systems, and their accurate simulation requires a rigorous event detection and restarting mechanism at every time instant in which switching occurs. This mechanism is computationally expensive, which results in prohibitively long simulation times when simulating the behaviour of even one or two instances of the switched DC-DC converter that comprise the SEH. To reduce simulation times and accelerate the modelling workflow, we considered the development of approximated linear models, herein continuous-time linearized models. This paper successfully demonstrates this approach in the scope of the Modelica® [18], [19] general purpose modelling language and validates it using Dymola® [20] Modelica tool and with electronic simulator package LTSpice® [21]. A continuous-time Linearized Model in Modelica (LZM), can be derived from the Switched Model in Modelica (SWM) by averaging of the converter model behaviour throughout the commutation cycle. The LZM and SWM simulation results are compared under the same boundary conditions, both during transient conditions and input voltage disturbances.

The models are implemented using the Modelica® object-oriented modeling language [19] within the Dymola® environment [20], using classes from the Modelica Standard Library (MSL) and VehicleInterfaces (VI) library [22]. Modelica® is a general purpose multiphysics modeling language which allows for integrated simulation of complex systems (mechanical, electrical, electronic, thermal, hydraulic, etc.)

The LZM simulation results are compared and validated using LTSpice®, a SPICE (Simulation Program with Integrated Circuits Emphasis) program [23], [24], purposely designed for high-speed simulations of mixed analog, digital, and switched electronic circuits. Equivalent circuits of the SWM model in buck and boost configurations are implemented in LTSpice®. These equivalent circuits constitute the LTSpice Switched Models (LTS). LTS simulation results are used as a reference for comparison and validation of the LZM models.

The Dymola® and LTSpice® simulation results are subjected to statistical analysis to evaluate the extent of similarity between both models. The Normalized Root Mean Square Error (NRMSE) is the test statistic of choice, implemented in Modelica® using the NRMSE computation module from [25].

The remainder of this article is structured as follows: Section II presents tools, materials and methods used. Within this section, Section II-A introduces the SWM model, whose components are sized according to power requirements of the motor for driving and regenerative braking; simulation times are determined as well. Section II-B introduces the linearized, continuous-time model (LZM) derived from the SWM and determines and compares simulation times against the SWM. Section III compares simulation results of the LZM and SWM and presents the validation of LZM simulation results against those of the LTS in LTSpice. Section IV presents conclusions of this work.

II. MATERIALS AND METHODS

The following software and libraries were used for the creation and simulation of SWM and LZM models:

1) Dymola (Dynamic Modeling Laboratory) - Version 2020 (64-bit) from Dassault Systèmes SE (France).
2) Modelica Standard Library - Version 3.2.3 from The Modelica Association.
3) VehicleInterfaces Library - Version 1.2.5 - Interface definitions and architectures for vehicle system modeling from The Modelica Association.

The following software was employed to create the LTS models used as a reference in the validation of LZM results:

1) LTspice XVII® (x64) from Analog Devices Corporation, Norwood, MA (USA)
2) LTspice standard libraries

Simulations were completed in a PC with the following specifications:

- Intel® Core™ i5-430 processor
- 4 GB DDR3 memory
- ATI Mobility Radeon HD5470, 512MB VRAM graphic card

In the following sections, the methods used in this work are presented.

A. SWITCHED DC-DC CONVERTER MODEL

The selected converter topology for this work is shown in Fig. 1. This corresponds to the well-known Non-isolated Half-Bridge Bidirectional DC-DC Converter (NBHBC), implemented in Modelica® with components from the MSL and the VI library.

A NBHBC results from the anti-parallel connection of a basic Boost and Buck DC-DC converters, adding the feature of bidirectional power flow [14]. This allows for operation in Boost mode in one direction and Buck mode in the other. In addition, non-isolated converters are lighter and more compact than their isolated counterparts due to the lack of transformers. In [14], a comparison between several topologies concludes that NBHBC has a reduced number of components with less device stress and less losses, making it a better alternative for use in lightweight EVs.

Out of the various converters that comprise the SEH, this work focuses on the main drive motor converter.

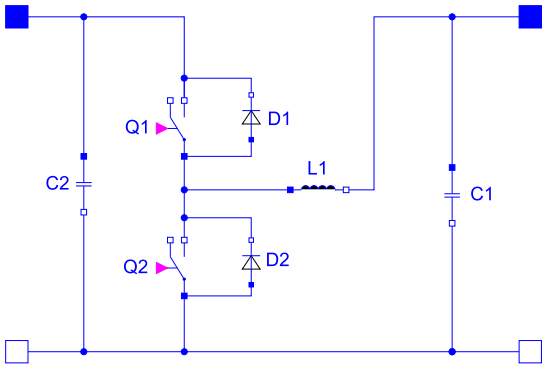

FIGURE 1. Non-isolated Half-Bridge converter Modelica model.

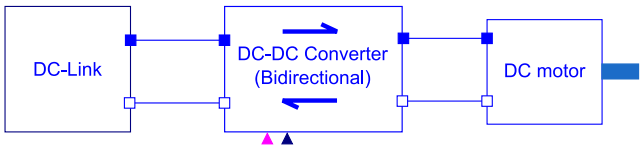

FIGURE 2. Schematic DC-Link and motor connection Modelica Model.

This converter must be bi-directional: in Buck mode it powers the motor from the DC-Link and in Boost mode it powers the DC-Link through regenerative braking.

A 250W motor, typically used by lightweight EVs such as bicycles and tricycles for city and inter-city travel on gentle slopes, was selected for converter dimensioning and specification [26]. The specifications of the Heinzmann Classic RN 120 e-bike wheel hub drive motor are used as a reference, with rated power 250W and 36 Vdc rated input voltage [27].

A nominal DC-Link voltage of 48 Vdc is specified. This voltage complies with the Low Voltage Directive (LVD) (2014/35/EU) and enables the employment of cables of smaller cross-section and weight in the vehicle. As previously explained, the converter operates in Buck mode when it feeds power to the main drive motor from the DC-Link. This mode of operation is justified by the fact that the converter can accommodate a wider range of voltages at the output in Buck mode, ranging from almost 0 up to the nominal voltage of the motor. See Fig. 2.

The DC-Link voltage range is established as 38-48 Vdc. The selected range is sufficiently broad to implement energy management strategies such as bus signalling, where the operation mode of the DC-DC converters in the SEH varies with the DC-Link voltage level.

The converter operates in Boost mode during regenerative braking, feeding energy to the DC-Link. The drive motor output voltage range is established to be between 6-36 Vdc, which means the converter will only recover energy for motor output voltages higher than 6 Vdc (6 Vdc equals to 4.3 km/h for a 26" e-bike tire - ERTRO 47-559). Motor output voltage is proportional to motor speed, and since at low vehicle speeds the available kinetic energy is low, harvesting energy at voltages lower than 6 Vdc does not justify the required increase in converter component size due to inductance.

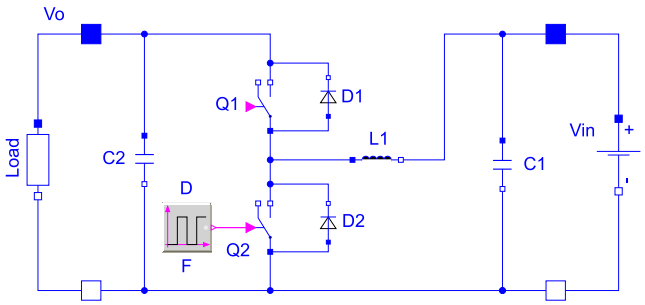

FIGURE 3. Half-Bridge converter in Boost mode.

TABLE 1. Main drive motor converter design specifications (Boost mode).

Var.	Description	Unit	Value
Po	Max. continuous output power	W	250
Vo	DC output High Voltage (HV)	V	48
Vi	DC input Low Voltage (LV) range	V	6-36
rI	Max. inductor current ripple ratio	–	0.40
rV	Max. output voltage ripple	–	0.05
F	Switching frequency	kHz	100

The switch from energy input to energy harvesting of the motor takes place either upon lifting of the accelerator pedal or when the brakes are applied, as long as the motor output voltage is greater than 6 Vdc.

The maximum inductor current ripple ratio and maximum output voltage ripple values are set at 40% and 5% respectively, using [28] and [14] as reference. Switching frequency is set at 100 kHz in accordance with [6], [29], [30] for hard-switching [6] low-power DC-DC converters, considering that higher frequencies lead to smaller inductances, albeit also incurring reduced efficiencies, increased power losses, RF noise and EMI. Converter component calculations and sizing were carried using the formulas proposed by [13], [28] and [14].

1) BOOST MODE

The Boost mode configuration is shown in Fig. 3. Here, the Q1 switch is permanently open, while Q2 commutates at fixed frequency F. Input voltage Vin is increased to the output voltage Vo by varying the duty cycle (D) of Q2.

Table 1 shows the design parameter specifications for the selected converter in Boost mode.

In Boost mode, the most unfavorable operation case is for $Vimin = 6$V [28]. The formulas used for component sizing are:

$$Vi = Vimin \tag{1}$$

$$Von = Vi \tag{2}$$

$$D = \frac{(Vo - Vi)}{Vo} \tag{3}$$

$$IL = \frac{Io}{(1 - D)} \tag{4}$$

$$Lmin = \frac{Von \cdot D}{(rI \cdot IL \cdot F)} \tag{5}$$

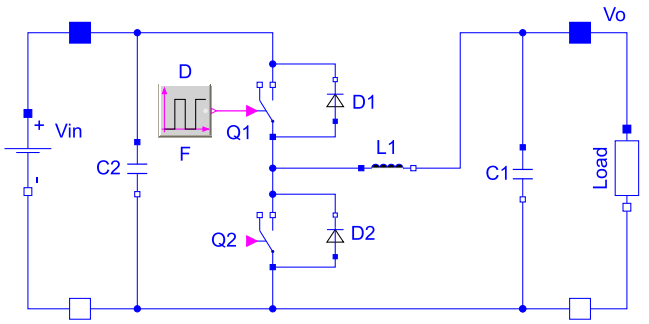

FIGURE 4. Half-Bridge converter in Buck mode.

TABLE 2. Main drive motor converter design specifications (Buck mode).

Var.	Description	Unit	Value
Po	Max. continuous output power	W	250
Vo	DC output LV range	V	6-36
Vi	DC input HV range	V	38-48
rI	Max. inductor current ripple ratio	–	0.40
rV	Max. output voltage ripple	–	0.05
F	Switching frequency	kHz	100

$$Cmin = \frac{Io \cdot D}{(F \cdot rV \cdot Vo)} \tag{6}$$

Which yielded the following results:

- $LminBoost = 3.15 \cdot 10^{-6}$ H
- $CminBoost = 1.8989 \cdot 10^{-5}$ F

Where,

- *Vimin*, minimum input voltage
- *Von*, voltage across the inductor while the switch is closed
- *D*, duty cycle. Ratio of the on-time of the switch to the time period
- *IL*, average inductor current
- *Io*, average load current
- *Lmin*, minimum inductor size (in Boost or Buck mode)
- *Cmin*, minimum capacitor size (in Boost or Buck mode)
- *L*, inductor size
- *C*, capacitor size
- *Rl*, Direct Current Resistance (DCR) for inductors.
- *Rc*, Equivalent Series Resistance (ESR) for capacitors.

2) BUCK MODE

The Buck mode configuration is shown in Fig. 4. In this case, Q2 is permanently open, while Q1 commutates at fixed frequency F. *Vin* is reduced to the required values of *Vo* as a function of the duty cycle (D) of Q1.

Table 2 shows the design parameter specifications for the selected converter in Buck mode.

In Buck mode, the most unfavorable operation case (for inductor and capacitor sizing) is for $Vimax = 48$V [28]. The formulas used in the design and operation are:

$$Vi = Vimax \tag{7}$$

$$Von = Vi - Vo \tag{8}$$
$$D = \frac{Vo}{Vi} \tag{9}$$
$$IL = \frac{Io}{(1-D)} \tag{10}$$
$$Lmin = \frac{Von \cdot D}{(rI \cdot IL \cdot F)} \tag{11}$$
$$Cmin = \frac{Io \cdot D}{(F \cdot rV \cdot Vo)} \tag{12}$$

Which yielded the following results:

- $LminBuck = 8.1052 \cdot 10^{-6}$ H
- $CminBuck = 2.8917 \cdot 10^{-5}$ F

3) INDUCTOR AND CAPACITOR CALCULATION AND SELECTION

The largest calculated values for Buck and Boost modes were used for inductor and capacitor sizing, and selection. The closest standardized values that were higher than the calculated values were selected.

For the inductor:

$$\begin{aligned} L &= max[LminBoost, LminBuck] \\ &= max[3.15 \cdot 10^{-6}, 8.1052 \cdot 10^{-6}] \\ &= 8.1052 \cdot 10^{-6} H \end{aligned} \tag{13}$$

The closest commercially available standard value which was higher than the calculated value was 8.2E-06 H [31]. Examples of commercially available inductors with these characteristics are CWS E70340-013 and CWS HF467-260M-45AH [32]. DCR for these inductors ranges from 2 to 3 mΩ. We therefore set Rl = 0.003 Ω.

For the capacitor:

$$\begin{aligned} C &= max[CminBoost, CminBuck] \\ &= max[1.8989 \cdot 10^{-5}, 2.8917 \cdot 10^{-5}] \\ &= 2.8917 \cdot 10^{-5} F \end{aligned} \tag{14}$$

The closest commercially available standard value is $56 \cdot 10^{-6}$ F = 56 μF; this value was selected. Examples of commercially available capacitors with these characteristics are Panasonic EEHAZF1H560 [33] and Kemet A767 [34].

The ESR for these capacitors ranges are 0.029 to 0.035 Ω at 100 kHz. We therefore chose Rc = 0.035 Ω.

B. LINEARIZED DC-DC CONVERTER MODEL

The previous section states that large simulation times are expected for the SWM. Hence, an equivalent dynamic model that allows for faster simulations is required, and which must be valid for Buck and Boost modes.

References [35] and [36] introduce a methodology for developing state-space linearized models, based on a method for modeling switching-converter power stages as a linear model of state-space descriptions of the switched networks.

In Cuk's PhD thesis [36] Part 1 (Continuous Conduction Mode), Chapter 3 (State Space Averaging, Hybrid Modeling and Circuit Averaging) the linearization formulas are derived.

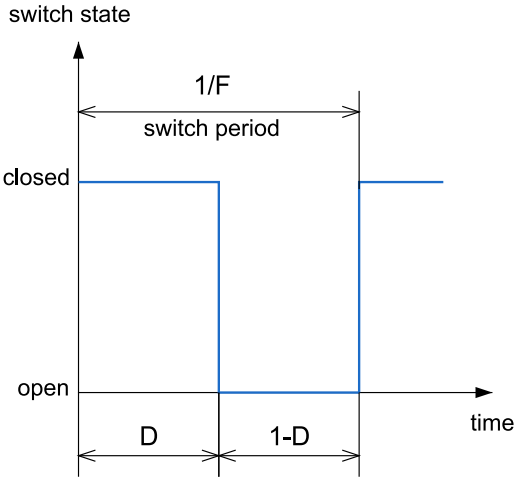

FIGURE 5. Definition of the two switched intervals D and 1-D.

A general state-space averaging method is developed for any DC-DC switching converter, and this is later specifically applied to a Boost converter, accounting for parasitic effects of the inductor and capacitor. These equations represent both the steady-state and dynamic behaviour of the converter. The transfer functions are derived from these, and later also specifically applied to a Boost converter. The basic operating principle of DC-DC converters is the fast commutation between two linear networks. Thus, assuming Continuous Conduction Mode (CCM) operation, where current through the inductor never drops to zero, only two discrete states exist for the circuit. A continuous-time representation of the switch state during one commutation cycle is displayed in Fig. 5.

Each time interval corresponds to one of the possible circuit configurations. State equations (15, 16) apply for the D interval, and equations (17, 18) for the $1 - D$ interval:

$$\dot{x} = A_1 \cdot x + b_1 \cdot V_{in} \tag{15}$$
$$y_1 = c_1^T \cdot x \tag{16}$$
$$\dot{x} = A_2 \cdot x + b_2 \cdot V_{in} \tag{17}$$
$$y_2 = c_2^T \cdot x \tag{18}$$

where,

- V_{in}, input voltage

The voltage across the capacitors (V_c) and the current through the inductors (i_L) are set as state variables. The total number of storage energy elements determines the order of the system. Therefore, the NBHBC is a second-order system for Buck and Boost configurations.

Once the state-space descriptions for the two possible converter states throughout the cycle time have been derived, these are replaced by a single state-space description that approximately represents the circuit behaviour across a full commutation cycle time. This is achieved through a weighted average of the effect of each state-space in proportion to their duration within the cycle. It is assumed these proportions remain unchanged within the same cycle.

The proposed NBHBC works in Boost or Buck mode depending on the direction in which current flows. Therefore, one linearized model is required for each of these configurations.

The SWM component values obtained in II-A3 were assigned to the linearized models. Since the coefficients in Equations (21) and (24) account for parasitic capacitor and inductor resistances, these were set as $R_l = 0.003\Omega$ and $R_c = 0.035\Omega$, which were the values previously employed in the SWM models (Fig. 3 and 4).

1) LINEARIZED BOOST MODE

Using the Boost circuit architecture in Fig. 3, the averaged state-space equations for a Boost converter (19) can be found in [35] and [36]:

$$\begin{aligned} \dot{x} &= A \cdot x + b \cdot V_{in} \\ x &= \begin{bmatrix} i_L \\ V_c \end{bmatrix} \\ \dot{x} &= \begin{bmatrix} \frac{di_L}{dt} \\ \frac{dV_c}{dt} \end{bmatrix} \\ y &= c^T \cdot x \\ y &= [V_o] \end{aligned} \tag{19}$$

where,

- V_o, output voltage.
- i_L, current through the inductors.
- V_c, voltage across the capacitors.

The averaged coefficients are (20):

$$\begin{aligned} A &= D \cdot A_1 + (1-D) \cdot A_2 \\ b &= D \cdot b_1 + (1-D) \cdot b_2 \\ c^T &= D \cdot {c_1}^T + (1-D) \cdot {c_2}^T \end{aligned} \tag{20}$$

which are obtained from the coefficients for each of the circuit states (21):

$$\begin{aligned} A_1 &= \begin{bmatrix} -\frac{R_l}{L} & 0 \\ 0 & -\frac{1}{(R+R_c)C} \end{bmatrix} \\ A_2 &= \begin{bmatrix} -\frac{R_l + R_c \parallel R}{L} & -\frac{R}{L(R+R_c)} \\ \frac{R}{(R+R_c)C} & -\frac{1}{(R+R_c)C} \end{bmatrix} \\ b_1 &= b_2 = \begin{bmatrix} \frac{1}{L} \\ 0 \end{bmatrix} \\ {c_1}^T &= \begin{bmatrix} 0 & \frac{R}{R+R_c} \end{bmatrix} \\ {c_2}^T &= \begin{bmatrix} R \parallel R_c & \frac{R}{R+R_c} \end{bmatrix} \end{aligned} \tag{21}$$

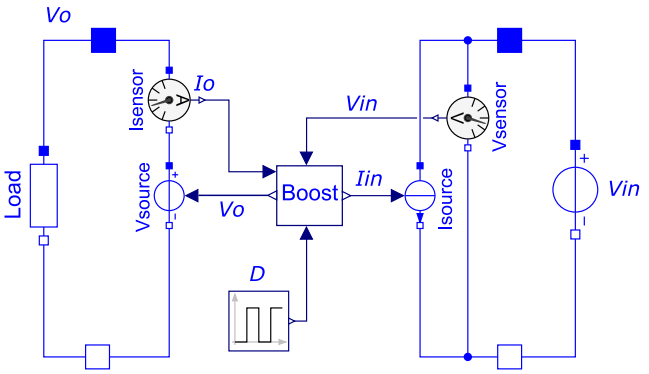

FIGURE 6. Schematic linearized Boost converter Modelica model.

where:

$$\frac{1}{R_c \parallel R} = \frac{1}{R_c} + \frac{1}{R} \tag{22}$$

Equations describing the relationship between input (I_{in}) and output (I_o) converter current (23) can be found in [36] and [37].

$$I_{in} = D \cdot I_o \tag{23}$$

These equations can be grouped inside a Modelica functional block, resulting in the Boost mode linearized model in Fig. 6.

2) LINEARIZED BUCK MODE

For this model, the Buck circuit architecture in Fig. 4 will be used. The coefficients for each of the circuit states in (24) are derived from [38], adding the effet of parasitic resistances as in boost mode. The averaged coefficients for each of the circuit states (20) and averaged state-space equations (19) can then be subsequently obtained for the Buck converter:

$$\begin{aligned} A_1 = A_2 &= \begin{bmatrix} -\frac{R_l + R_c \parallel R}{L} & -\frac{R}{L(R+R_c)} \\ \frac{R}{(R+R_c)C} & -\frac{1}{(R+R_c)C} \end{bmatrix} \\ b_1 &= \begin{bmatrix} \frac{1}{L} \\ 0 \end{bmatrix} \\ b_2 &= \begin{bmatrix} 0 \\ 0 \end{bmatrix} \\ {c_1}^T = {c_1}^T &= \begin{bmatrix} R \parallel R_c & \frac{R}{R+R_c} \end{bmatrix} \end{aligned} \tag{24}$$

As with the Boost mode linearized model, these equations can be grouped within a functional block, which gives the linearized Buck model in Fig. 7.

III. RESULTS AND DISCUSSION

A. SIMULATION TIME REQUIREMENTS

As indicated in the introduction, each component in the SEH requires a converter that adapts the output voltage of said component to that of the DC-Link and vice-versa.

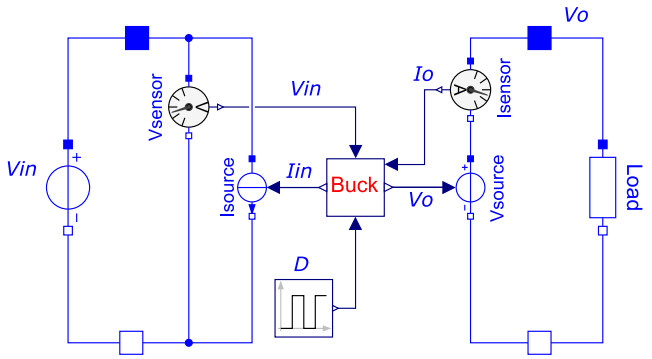

FIGURE 7. Schematic linearized Buck converter Modelica model.

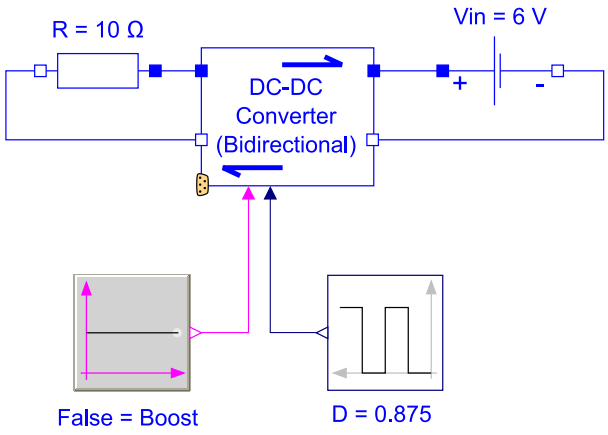

FIGURE 8. Switched converter model on Boost mode. Vin = 6V, Vout = 48V.

The number of converters in the SEH will therefore equal the number of components that comprise it. This could pose a significant computational expense and therefore it is necessary to evaluate and define maximum simulation times for the selected converter models.

1) SWM SIMULATION TIME REQUIREMENTS

Since the SWM circuit structure is modified each time the state of a switch changes, it is necessary to re-initialize the model equations at twice the commutation frequency F, which can be used to estimate the necessary computational load. Two models of the SWM converter, one in Boost mode and another in Buck mode, were used to evaluate simulation times. Both models were comprised of an ideal voltage input source and an output resistance load.

a: BOOST MODE

The Boost mode configuration is portrayed in Fig. 8. The least favourable conditions of $Vin = 6$ V, $Vout = 48$ V were selected. An output load of 10Ω was selected, providing an output power of 230W at 48V, which is lower than the 250W power specification of the converter. The required duty cycle was calculated using Equation (3).

$$D = \frac{48 - 6}{48} = 0.875 \tag{25}$$

A 1 s simulation was run in Dymola, using the DASSL integration method (DAE Multi-Step Solver (dassl/dasslrt of Petzold modified by Dassault Systemes)), yielding the following results:

Log-file of program ./dymosim (generated: Mon Jun 10 20:24:41 2019) ...
"SwitchedConverterBoostEval_100k_RcRl.mat" creating (simulation result file) ...
Integration started at $T = 0$ using integration method DASSL
(DAE multi-step solver (dassl/dasslrt of Petzold modified by Dassault Systemes))
Integration terminated successfully at $T = 1$
CPU-time for integration : 48.5 seconds
...
Number of result points : 400502
...
Number of accepted steps : 2298718
Number of f-evaluations (dynamics) : 2697841
Number of crossing function evaluations : 3427286
Number of Jacobian-evaluations : 2098622
...

That is, 48.5 s are needed for running a 1 s simulation.

b: BUCK MODE

The Buck mode configuration is portrayed in Fig. 9. The conditions of $Vin = 48$V, $Vout = 36$V were selected. An output load of 6 Ω was selected, which provides an output power of 216W at 36V, lower than the 250W power specifications. The required duty cycle was calculated using Equation (9):

$$D = \frac{36}{48} = 0.75 \tag{26}$$

This simulation was run for 1 s, yielding the following results:

Log-file of program ./dymosim (generated: Tue Jun 18 19:32:02 2019) ...
"SwitchedConverterBuckEval_100k_RcRl.mat" creating (simulation result file) ...
Integration started at $T = 0$ using integration method DASSL
(DAE multi-step solver (dassl/dasslrt of Petzold modified by Dassault Systemes))
Integration terminated successfully at $T = 1$
CPU-time for integration : 53.4 seconds
...
Number of result points : 400502
...
Number of accepted steps : 3697301
Number of f-evaluations (dynamics) : 5396364
Number of crossing function evaluations : 4740200
Number of Jacobian-evaluations : 2497915
...

A slightly longer simulation time of 53.4 s is needed for running a 1 s simulation.

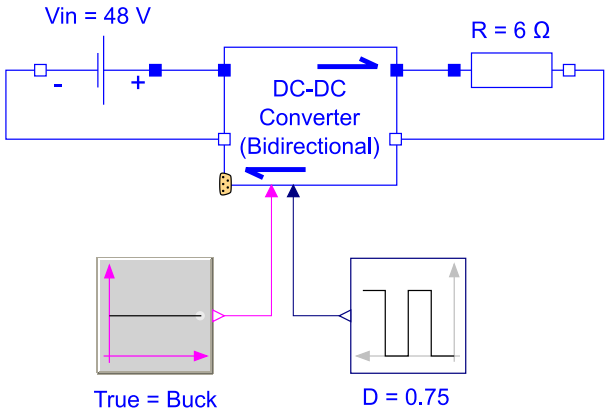

FIGURE 9. Switched converter model on Buck mode. Vin = 48V, Vout = 36V.

2) LZM SIMULATION TIME REQUIREMENTS

Simulation times were calculated for both Boost and Buck linearized models, applying the same boundary conditions as in the SWM (ideal voltage input source, linearized converter and output resistance load).

a: BOOST MODE

The same operating conditions were applied as in III-A1a to the linearized converter model in Fig. 6:

- $Vin = 6\text{V}$
- $Vout = 48\text{V}$
- $R = 10\Omega$
- $D = \dfrac{48-6}{48} = 0.875$

A 1 s simulation of this model was ran within Dymola using the DASSL integration method, yielding the following results:

Log-file of program./dymosim (generated: Tue Jun 18 20:01:39 2019) . . .
"HvLvAvgBoostEval_100k_RcRl_2.mat" creating (simulation result file) . . .
Integration started at T = 0 using integration method DASSL
(DAE multi-step solver (dassl/dasslrt of Petzold modified by Dassault Systemes))
Integration terminated successfully at T = 1
CPU-time for integration : 0.014 seconds
. . .
Number of result points : 502
. . .
Number of accepted steps : 176
Number of f-evaluations (dynamics) : 346
Number of Jacobian-evaluations : 31
. . .

The LZM Boost proposed model provided a simulation time of 0.014 s for running a 1 s, 3464 times faster than its SWM counterpart.

b: BUCK MODE

The same operating conditions were applied as in III-A1.b to the linearized converter model in Fig. 7:

- $Vin = 48\text{V}$
- $Vout = 36\text{V}$
- $R = 6\Omega$
- $D = \dfrac{36}{48} = 0.75$

Once again, a 1 s simulation of this model was ran within Dymola using the DASSL integration method, yielding the following results:

Log-file of program ./dymosim (generated: Tue Jun 18 20:25:38 2019)
. . .
"HvLvAvgBuckEval_100k_RcRl_2.mat" creating (simulation result file)
. . .
Integration started at T = 0 using integration method DASSL
(DAE multi-step solver (dassl/dasslrt of Petzold modified by Dassault Systemes))
Integration terminated successfully at T = 1
CPU-time for integration : 0.012 seconds
. . .
Number of result points : 502
. . .
Number of accepted steps : 338
Number of f-evaluations (dynamics) : 676
Number of Jacobian-evaluations : 40
. . .

For the proposed LZM Buck model, a simulation time of 0.012 s is needed for running a 1 s simulation, 4450 times faster than its SWM counterpart.

B. BEHAVIOUR COMPARISON AND VALIDATION OF SWITCHED AND LINEARIZED MODELS

This chapter is concerned with comparing and validating the proposed Buck and Boost LZM's model against their SWM equivalents. This comparison was carried in steady-state and dynamic operating conditions to assess their behaviour against disturbances.

The SWM and LZM models were compared under the same boundary conditions within a single simulation. Simulation results from the LTS model, equivalent to the SWM and implemented within LTSpice® specific purpose modeler, was later used for LZM model validation. LTSpice was chosen for validation due to the reliability of its results in the electronic domain.

During start-up conditions, the SWM (Boost, Buck) models presented in Fig. 8, 9 and LZM (Boost, Buck) models were compared under the same boundary conditions: Equal input voltage, resistance load, and duty cycle. LZM (Boost, Buck) models were validated against simulation results from

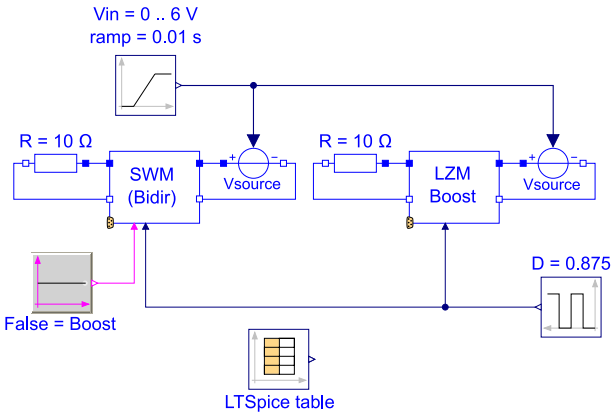

FIGURE 10. Modelica model for performance comparison between SWM, LZM and LTS Boost converter models during start-up conditions.

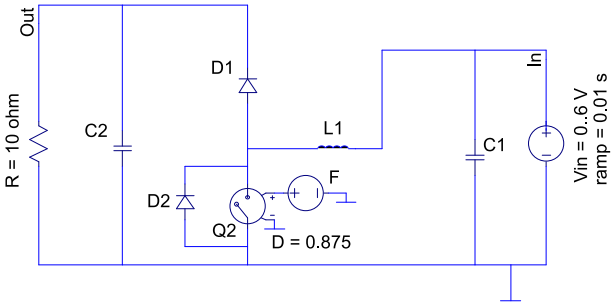

FIGURE 11. LTSpice Boost model during start-up conditions.

the LTS (Boost, Buck) models under the same boundary conditions as well (input voltage, resistance load and duty cycle).

During dynamic operation, the converter is subjected to disturbances in input voltage, load and duty cycle D (which is modified by the output voltage/current control system).

For simplicity, only the Boost configuration was dynamically simulated for disturbances in *Vin*, which is of critical importance when the motor harvests energy through regenerative braking.

The simulation results were subjected to statistical analysis to evaluate the extent of similarity between models. The Normalized Root Mean Square Error (NRMSE) was the test statistic of choice, implemented in Modelica® using the NRMSE computation module from [25].

1) COMPARISON AND VALIDATION DURING START-UP CONDITIONS

a: BOOST MODE

The model in Fig. 10 was used for comparison of the Boost converter model performance. The simulation ran for 0.03 s and parameters were 6 V input voltage with a 0.01 s linear ramp, 10Ω load and $D = 0.875$ for both models (SWM and LZM). Validation was executed through comparison with LTS model simulation results in LTSpice (Fig. 11), stored inside the LTSpice table in Fig. 10 model.

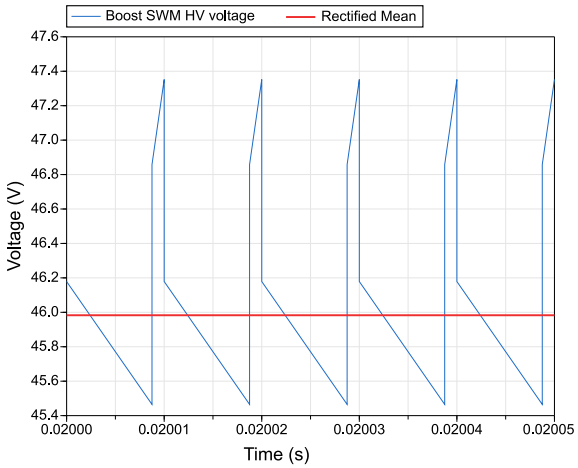

FIGURE 12. ARV computed from switched converter output voltage in steady state conditions.

The output voltage in the SWM and LTS models fluctuates at the commutation frequency, as seen in Fig. 12. To ensure an adequate comparison of results, it is necessary to use an averaged value of the output voltage. To achieve this, the RectifiedMean [39] function in Modelica was used. This function computes the Average Rectified Value (ARV), which is an averaged absolute value of a waveform over one full period of the waveform [40]. This is computed continuously for a $1 \cdot 10^{-5}$ s cycle time. NRMSE is computed for the time interval 0.01 to 0.03 s with sampling frequency of $1 \cdot 10^5$ Hz. This sample frequency was selected to obtain enough data to compute the NRMSE index, resulting in approximately $2 \cdot 10^3$ samples for the indicated interval. The same criteria are applied for subsequent computations of this index.

Simulation results are shown in Fig. 13. Graph (a) portrays the behaviour of all three models throughout the full simulation. Graph (b) displays the signal differences between SWM-LZM and LTS-LZM:

- (SWM-LZM) Once the output voltage has reached steady-state (LZM, 45.994 V t = 0.03 s), a difference of 9.55 mV (0.021%) is observed between the models. NRMSE reaches a value of 0.001115 at t = 0.03 s.
- (LTS-LZM) Once the output voltage has reached steady-state (LZM, 45.994 V t = 0.03 s), a difference of 844 mV (1.923%) is observed between the models. NRMSE reaches a value of 0.8665 at t = 0.03 s.

The results show negligible response differences between the SWM and LZM during start-up. The differences between LZM and LTS are small as well, albeit with a slight offset in output voltage that remains largely constant throughout the simulation. Furthermore, the transient response of all models is closely matched.

b: BUCK MODE

The model in Fig. 14 was used for assessment of the Buck converter model performance. The simulation ran for 0.03 s and parameters were 48 V input voltage with a 0.01 s linear ramp, 6Ω load and $D = 0.75$ for both models (SWM and

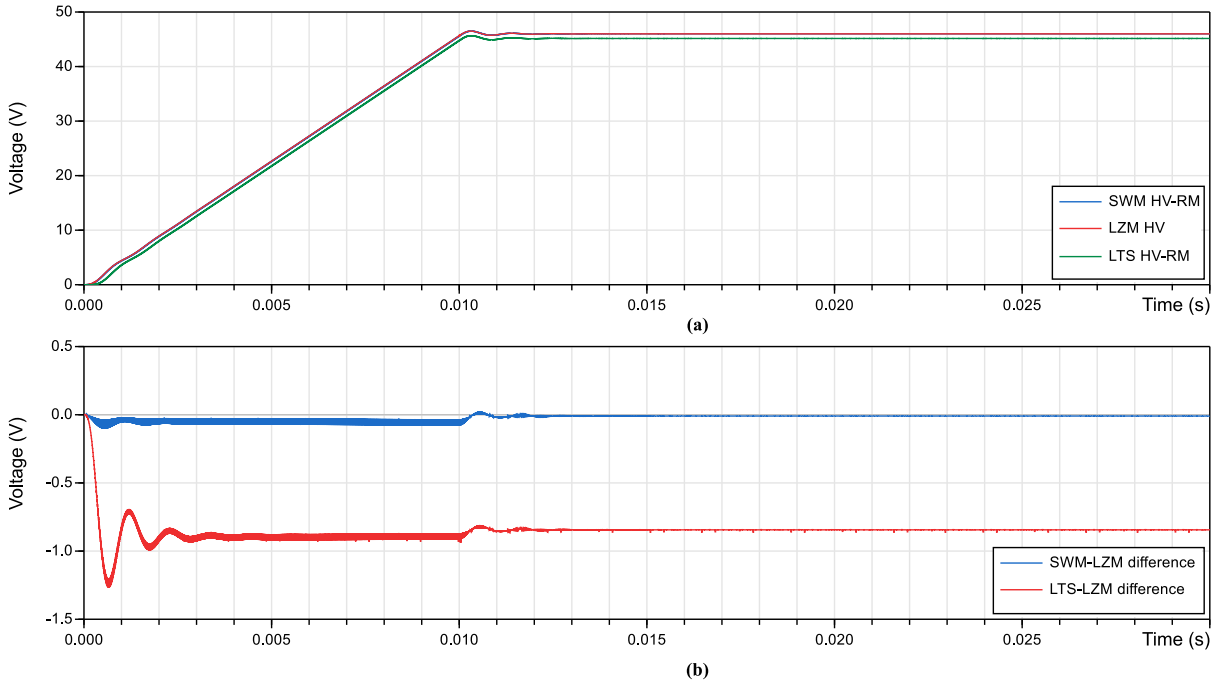

FIGURE 13. Output voltage comparison between SWM, LZM and LTS boost converter models in start-up conditions: (a) Output voltage. (b) Differences between SWM-LZM and LTS-LZM.

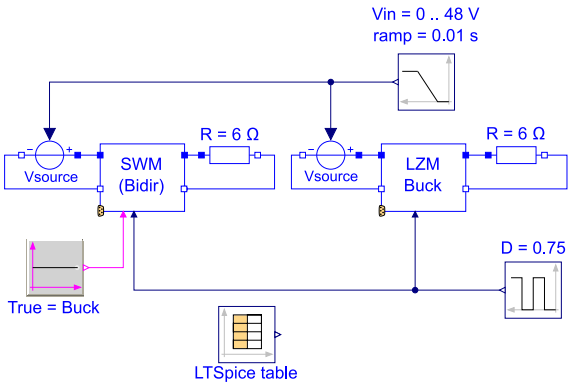

FIGURE 14. Modelica model for performance comparison between SWM, LZM and LTS Buck converter models in start-up conditions.

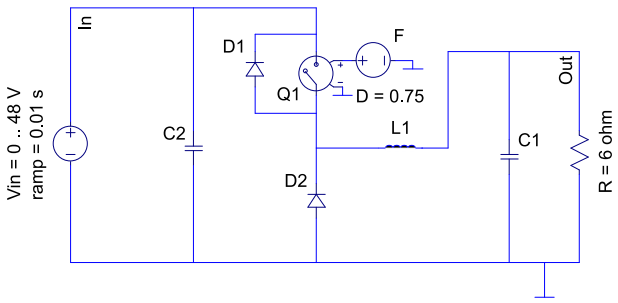

FIGURE 15. LTSpice Buck model in start-up conditions.

LZM). Validation was executed through comparison with LTS model simulation results in LTSpice (Fig. 15), stored inside the LTSpice table in Fig. 14 model.

As for the Boost model simulations, the output voltage in the SWM and LTS models fluctuates at the commutation frequency, hence it is necessary to use its averaged value. To achieve this, the RectifiedMean function in Modelica [39] is used again to compute the ARV [40]. This is computed continuously for a $1 \cdot 10^{-5}$ s cycle time. NRMSE is computed for the time interval 0.01 to 0.03 s with sampling frequency of $1 \cdot 10^5$ Hz.

Simulation results are shown in Fig. 16. Graph (a) portrays the behaviour of all three models throughout the full simulation. Graph (b) displays the signal differences between SWM-LZM and LTS-LZM:

- (SWM-LZM) Once the output voltage has reached steady-state (LZM, 35.982 V, t = 0.03 s), a difference of $6.68 \cdot 10^{-5}$ V (0.000185%) is observed between the models. NRMSE reaches a value of 0.001026 at t = 0.03 s.
- (LTS-LZM) Once the output voltage has reached steady-state (LZM, 35.982 V, t = 0.03 s), a difference of 197 mV (0.548%) is observed between the models. NRMSE reaches a value of 0.1973 at t = 0.03 s.

Results show that response differences are negligible during start-up and steady-state. Furthermore the transient response of all models is closely matched (Fig. 16), taking into account the reduced simulation times.

2) COMPARISON AND VALIDATION UNDER SINUSOIDAL DISTURBANCES

In this section, the Boost model responses to a variable input voltage source were measured for the SWM, LZM

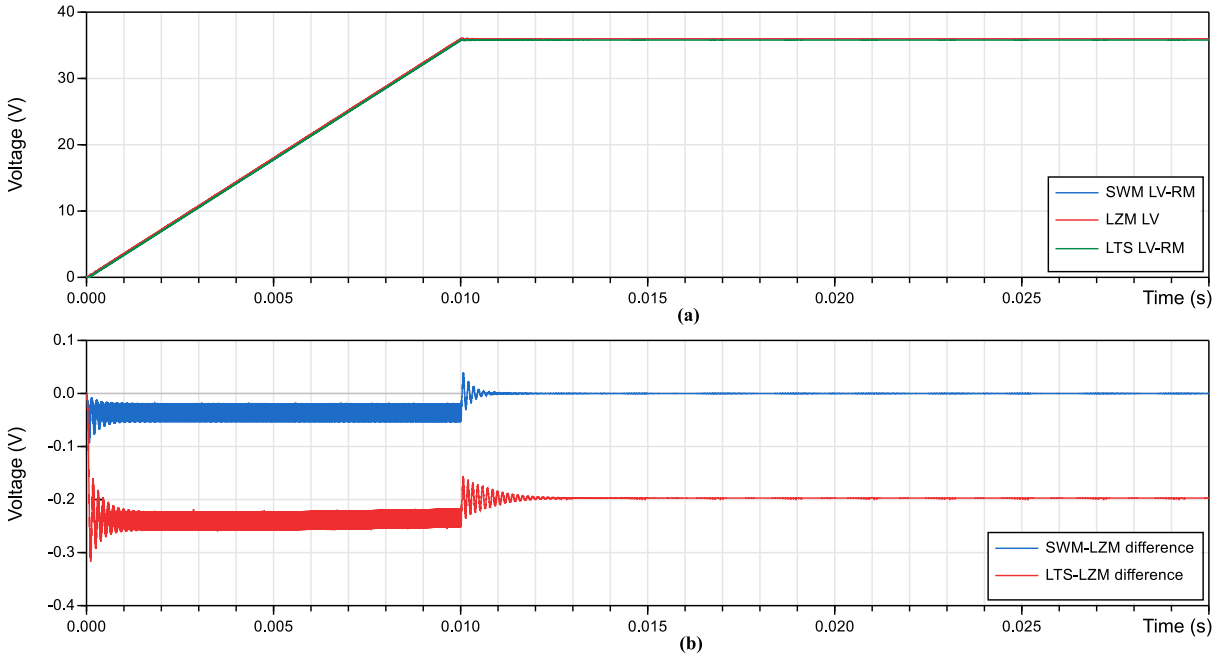

FIGURE 16. Output voltage comparison between SWM, LZM and LTS buck converter models during start-up conditions: (a) Output voltage. (b) Differences between SWM-LZM and LTS-LZM.

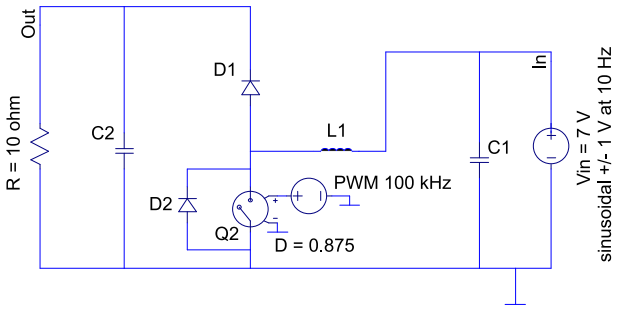

FIGURE 17. LTSpice boost model during sinusoidal supply voltage conditions.

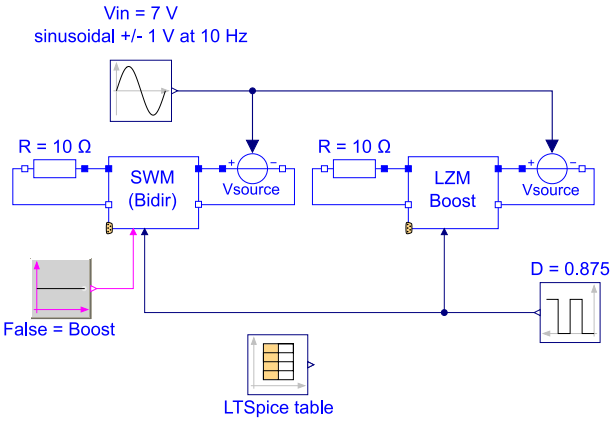

FIGURE 18. Modelica model including LTSpice results for comparison during sinusoidal supply voltage disturbance conditions.

and LTS. This variable input voltage source emulates energy harvesting during regenerative braking of the motor. The input voltage oscillates according to a sinusoidal function with a nominal value of 7 V, frequency of 10 Hz and amplitude of ±1 V. The voltage fluctuations were applied from t = 0.01 s to avoid oscillations from the starting transient region. The simulation ran for 0.3 s and parameters were 10Ω load and D = 0.875. The dynamic behaviour of the Boost LZM was validated against the LTS model simulation results.

As in the previous cases, the RectifiedMean function [39] was used to compute the ARV [40] of the output voltage for the SWM and LTS models. This is computed continuously for a $1 \cdot 10^{-5}$ s cycle time. NRMSE is computed for the time interval 0.01 to 0.3 s with sampling frequency of $1 \cdot 10^{5}$ Hz. Fig. 17 displays the Boost LTS model in LTSpice.

The model in Fig. 18 was used for comparison against LTSpice simulation results. Simulation results from the LTS model (Fig. 17) are stored inside the LTSpice table for the previously specified boundary conditions.

Simulation results are shown in Fig. 19 for the time interval 0.01 to 0.3 s. Graph (a) displays the output voltage behaviour for the SWM, LZM and LTS. Graph (b) illustrates the signal differences between SWM-LZM and LTS-LZM:

- (SWM-LZM) The differences in output voltage oscillate between −4.9 mV and −23.4 mV for the interval 0.01-0.3 s, resulting in a maximum difference of −0.0435% for an ARV voltage of 53.7 V. NRMSE reaches a value of 0.003165 at t = 0.03 s.
- (LTS-LZM) The differences in output voltage oscillate between −858 mV and −877 mV for the interval 0.01 to 0.3 s, resulting in a maximum difference of −1.633%

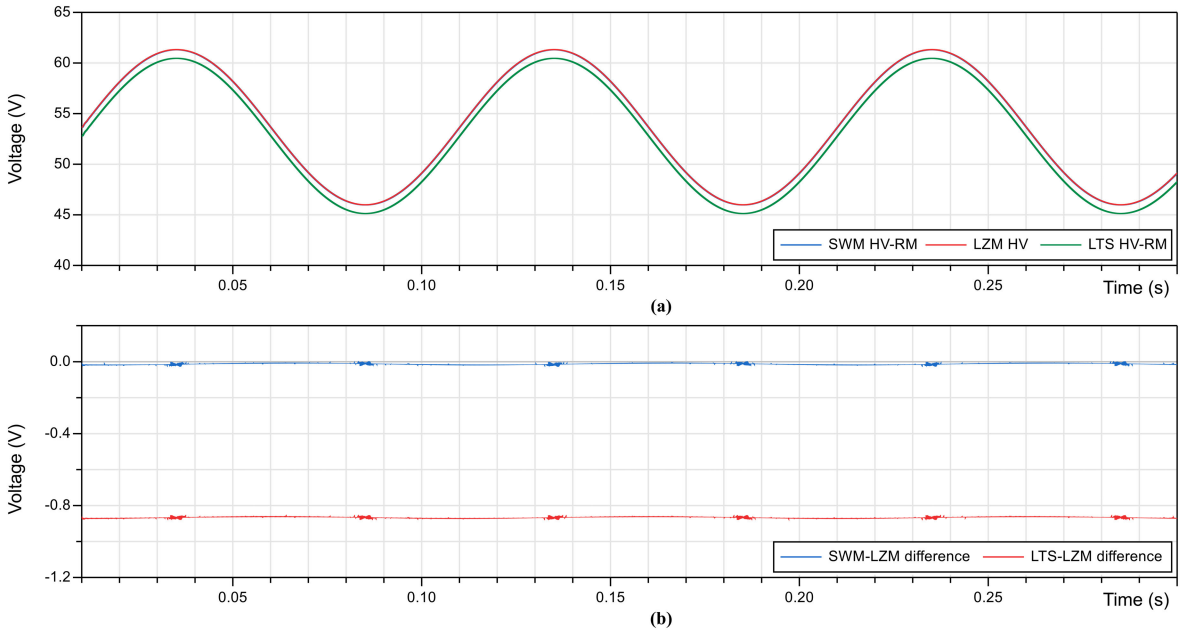

FIGURE 19. Performance comparison between SWM, LZM y LTS Boost converter models under sinusoidal supply voltage conditions: (a) Output voltage. (b) Differences between SWM-LZM and LTS-LZM.

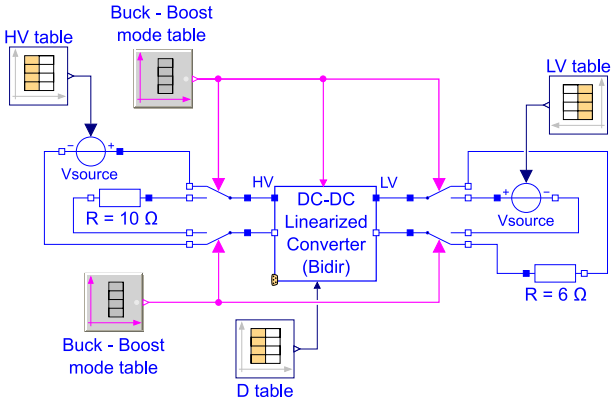

FIGURE 20. Bi-directional Buck-Boost Converter Modelica model.

for an ARV voltage of 53.7 V. NRMSE reaches a value of 0.2153 at t = 0.03 s.

These results show that differences in dynamic behaviour are negligible, even for significant fluctuations in input voltage. Differences between the SWM and LZM were slightly higher in sinusoidal disturbance than during start-up conditions, whereas the difference between LTS-LZM was smaller than in start-up conditions. Overall, results show that the LZM closely matches the behaviour of the reference LTS model whilst exhibiting 4450 times faster simulation times with respect to the SWM.

C. BIDIRECTIONAL CONVERTER

As previously mentioned in this work, a linearized NBHBC model is proposed for use in the main drive motor for energy input and harvesting. In previous sections the models were compared and validated for unidirectional operation (Boost and Buck mode). This paragraph demonstrates the ability of the LZM to operate in bi-directional Buck-Boost mode using a proposed cycle that alternates between the two modes.

TABLE 3. Bi-directional Buck-Boost Converter operating cycle.

Time (s)	Mode	D	HV (V)	LV (V)
0	Buck	0.5	48	–
2	Buck	0.75	48	–
4	Boost	0.625	–	18
6	Boost	0.75	–	12
8	Boost	0.875	–	6
10	Buck	0.75	48	–

A bi-directional Buck-Boost commutable converter model (Fig. 20) can be obtained by combining the LZMs (Boost and Buck mode) proposed in II-B. This model was used to simulate bi-directional behaviour.

During Buck mode operation, a constant input voltage of 48 V is applied to simulate the nominal voltage of the SEH, as well as a 6 Ω constant load and a variable D to obtain a variety of output voltages. During Boost mode operation, the output voltage must always match the nominal voltage in the SEH. Therefore, D is continuously adjusted using Equation (3). A static output load of 10 Ω is set. Table 3 summarizes the proposed cycle of operation.

The simulation results are displayed in Fig. 21. Graph (**a**) shows HV and LV converter voltages throughout the operating cycle, Graph (**b**) exhibits D values and Graph (**c**)

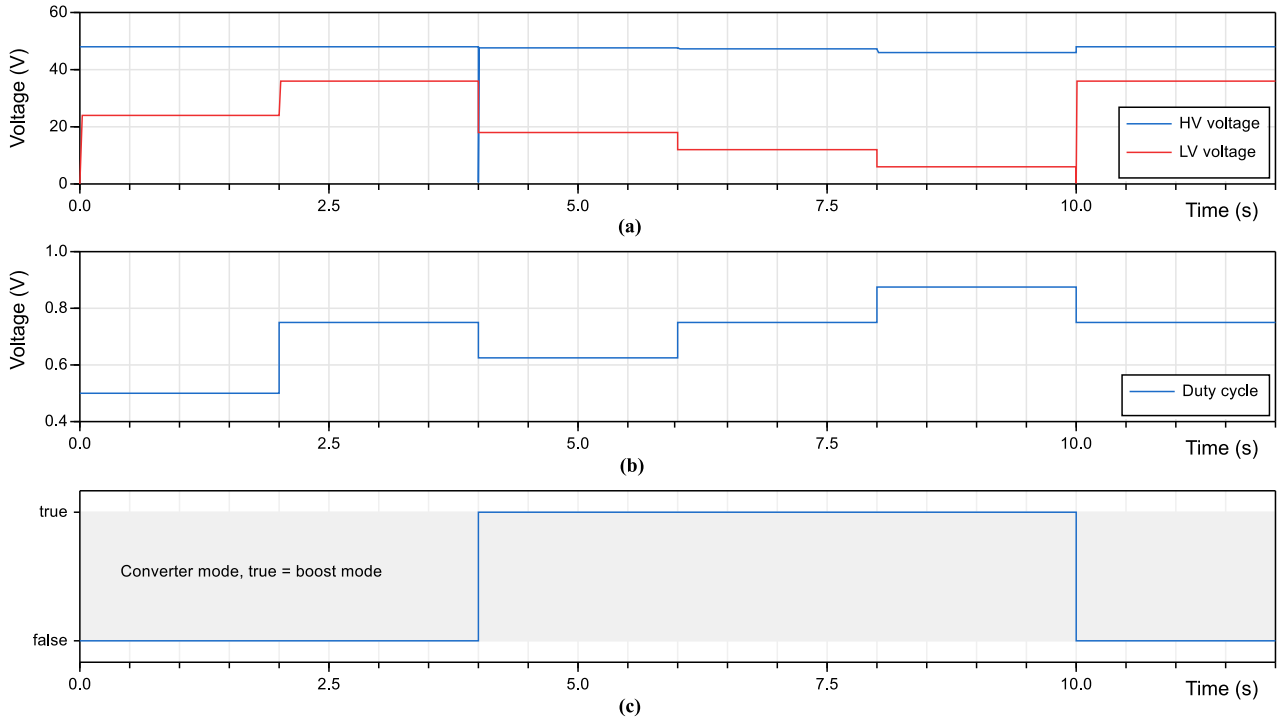

FIGURE 21. Bidirectional buck-boost converter simulation for the operating cycle proposed in Table 3: (a) LV & HV converter voltage. (b) Duty-cycle converter values. (c) Bi-directional converter mode.

displays the converter mode (Buck/Boost) at each stage of the operational cycle. This 12 s simulation was completed by the LZM model in only 1 s, which proves the possibility of using several instances of this model in a complete SEH model with reduced simulation times.

Log-file of program ./dymosim (generated: Mon Nov 11 23:28:48 2019)

...

"BiDirLZM_100k_cycle1.mat" creating (simulation result file)

...

Integration started at T = 0 using integration method DASSL
(DAE multi-step solver (dassl/dasslrt of Petzold modified by Dassault Systemes))

...

Integration terminated successfully at T = 12
CPU-time for integration : 1 *seconds*

...

IV. CONCLUSION

The results obtained in section III-A2 show that simulation times drop from 48.5 s in the SWM to 0.014 s in the LZM for a 1 s simulation in Boost mode, and from 53.4 s to 0.012 s in Buck mode. Hence, the LZM yields simulation runs that are between 3464 and 4450 times faster than the SWM. This also implies that LZM simulations run between 71 and 83 times faster than real-time with the hardware used for this research. Interpolation of results indicates that an ECE15 [41] standardized urban driving simulation cycle (195 s) would be complete in 2.535 s.

Results in Section III-B show that the LZM behaviour closely matches the LTS reference model under both start-up and sinusoidal supply voltage disturbance conditions.

During start-up conditions, the following results were obtained (Section III-B1):

- In Boost mode, the LZM and LTS exhibited very similar transient responses with a small, constant offset throughout the simulation. Once the output voltage had reached steady-state (LZM,45.994 V at t = 0.03 s) this constant offset amounted for a difference of 844 mV (1.923%) between the models. For these simulations, NRMSE = 0.8665 at t = 0.03 s.
- In Buck mode, the LZM and LTS once again showed very similar transient responses with a small, constant offset throughout the simulation. Once the output voltage had reached steady-state (LZM,35.982 V at t = 0.03 s) this constant offset amounted to a difference of 197 mV (0.548%) between the models. For these simulations, NRMSE = 0.1973 at t = 0.03 s.

During Boost mode operation with sinusoidal supply voltage disturbances (amplitude 1 V, 10 Hz), the following results were obtained (Section III-B2):

- Dynamic behaviour was very similar for the LTS and LZM simulations, exhibiting a small offset throughout the simulation. Furthermore, these differences were less significant than for the start-up simulations.

- The offset was observed to oscillate between −858 mV and −877 mV between t = 0.01 s and t = 0.3 s, yielding a maximum difference between the simulations of −1.633% for ARV = 53.7 V. In these simulations, NRMSE = 0.2153 at t = 0.03 s.

REFERENCES

[1] United Nations Environment Programme, "Hybrid Electric Vehicles: An overview of current technology and its application in developing and transitional countries," United Nations Environ. Programme, Nairobi, Kenya, Tech. Rep., 2009. [Online]. Available: http://www.unep.org/transport/pcfv/PDF/HEV_Report.pdf

[2] *Transport, Energy CO_2—Moving Toward Sustainability*. Paris, France: IEA, 2009. [Online]. Available: http://www.iea.org/publications/freepublications/publication/transport2009.pdf

[3] E. Commission, *A Sustainable Future for Transports—Towards an Integreated Technology-Led User-Friendly System*. Luxembourg, Europe: Office of the European Union, 2009.

[4] F. Gomez, L. Yebra, and A. Giménez, "Modelling a smart-grid for a solar powered electric vehicle," in *Proc. 9th Vienna Conf. Math. Modeling*, vol. 55. Vienna, Austria: ARGESIM Publisher, 2018, pp. 5–6. [Online]. Available: https://www.asim-gi.org/fileadmin/user_upload_argesim/ARGESIM_Publications_OA/MATHMOD_Publications_OA/MATHMOD_2018_AR55/articles/a55113.arep.55.pdf

[5] L. Martinez Salamero, A. Cid-Pastor, A. El Aroudi, R. Giral, and J. Calvente, "Modelado y control de convertidores conmutados continua-continua: Una perspectiva tutorial," *Revista Iberoamericana de Automática e Informática Ind. RIAI*, vol. 6, no. 4, pp. 5–20, Oct. 2009. [Online]. Available: http://linkinghub.elsevier.com/retrieve/pii/S1697791209701049

[6] D. Czarkowski, "DC–DC converters," in *Power Electronics Handbook*, 4th ed. M. H. Rashid, Ed. Oxford, U.K.: Butterworth-Heinemann, 2018, ch. 10, pp. 275–288. [Online]. Available: http://www.sciencedirect.com/science/article/pii/B9780128114070000106

[7] J. Chen, D. Maksimovic, and R. Erickson, "Buck-boost PWM converters having two independently controlled switches," in *Proc. IEEE 32nd Annu. Power Electron. Spec. Conf.*, vol. 2, Jun. 2001, pp. 736–741.

[8] F. Caricchi, F. Crescimbini, F. G. Capponi, and L. Solero, "Study of bidirectional buck-boost converter topologies for application in electrical vehicle motor drives," in *Proc. 13th Annu. Appl. Power Electron. Conf. Exposit. (APEC)*, vol. 1, 1998, pp. 287–293.

[9] M. G. Valencia and A. A. Gomez, "Diseño estático de un convertidor DC/DC reductor-elevador bidireccional," *Tecnura*, vol. 14, no. 26, pp. 7–14, 2010. [Online]. Available: http://revistas.udistrital.edu.co/ojs/index.php/Tecnura/article/view/6682

[10] J.-K. Shiau and C.-W. Ma, "Li-ion battery charging with a buck-boost power converter for a solar powered battery management system," *Energies*, vol. 6, no. 3, pp. 1669–1699, 2013. [Online]. Available: http://www.mdpi.com/1996-1073/6/3/1669/

[11] M. Hedlund, "Design and construction of a bidirectional DCDC converter for an EV application," Ph.D. dissertation, Uppsala Univ., Uppsala, Sweden, 2010. [Online]. Available: http://uu.diva-portal.org/smash/record.jsf?searchId=5&pid=diva2%3A301346&dswid=-590 and http://www.teknik.uu.se/electricity/publications/Publications_2000-2014/#2010

[12] H. Qiao, Y. Zhang, Y. Yao, and L. Wei, "Analysis of buck-boost converters for fuel cell electric vehicles," in *Proc. IEEE Int. Conf. Veh. Electron. Saf. (ICVES)*, Dec. 2006, pp. 109–113.

[13] K. T. Ahmed, M. Datta, and N. Mohammad, "A novel two switch non-inverting buck-boost converter based maximum power point tracking system," *Int. J. Elect. Comput. Eng.*, vol. 3, pp. 467–477, May 2013. [Online]. Available: http://iaesjournal.com/online/index.php/IJECE/article/view/2772

[14] R. M. Schupbach and J. C. Balda, "Comparing DC-DC converters for power management in hybrid electric vehicles," in *Proc. IEEE Int. Electric Mach. Drives Conf. (IEMDC)*, Jun. 2003, pp. 1369–1374. [Online]. Available: http://ieeexplore.ieee.org/lpdocs/epic03/wrapper.htm?arnumber=1210630

[15] Y.-L. Ke, Y.-C. Chuang, and H.-S. Chuang, "Energy recovery electric bicycle with two-quadrant DC motor drivers," in *Proc. IEEE Ind. Appl. Soc. Annu. Meeting*, Oct. 2009, pp. 1–7. [Online]. Available: http://ieeexplore.ieee.org/lpdocs/epic03/wrapper.htm?arnumber=5324928

[16] M. C. Joshi, S. Samanta, and G. Srungavarapu, "Battery ultracapacitor based DC motor drive for electric vehicles," in *Proc. IEEE Region 10 Symp. (TENSYMP)*, Jul. 2017, pp. 1–5. [Online]. Available: https://ieeexplore–ieee–org.ual.debiblio.com/stamp/stamp.jsp?tp=&arnumber=8070057

[17] F. Gomez, L. Yebra, A. Gimenez, and J. Torres-Moreno, "Modelling of batteries for application in light electric urban vehicles," *Revista Iberoamericana de Automática e Informática Ind.*, vol. 16, no. 4, pp. 459–466, 2019. [Online]. Available: https://polipapers.upv.es/index.php/RIAI/article/view/10609

[18] H. Olsson *et al.*, "Modelica—A unified object-oriented language for systems modeling. Language specification. version 3.4," Modelica Assoc., Linköping, Sweden, Tech. Rep., Apr. 2017. [Online]. Available: https://www.modelica.org/documents/ModelicaSpec34.pdf

[19] P. Fritzson, *Principles of Object-Oriented Modeling and Simulation With Modelica 3.3: A Cyber-Physical Approach*, 2nd ed. Linköping, Sweden: Wiley, 2015. [Online]. Available: https://books.google.es/books?id=wgIaBgAAQBAJ

[20] D. S. Ab, "Dymola—Dynamic modeling laboratory—User manual," Lund, Sweden, 2018, p. 847. [Online]. Available: http://www.dymola.com

[21] *Ltspice, One Technology Way*. Analog Devices, Norwood, MA, USA, 2020. [Online]. Available: https://www.analog.com/en/design-center/design-tools-and-calculators/ltspice-simulator.html

[22] M. Dempsey, M. Gäfvert, P. Harman, C. Kral, M. Otter, and P. Treffinger, "Coordinated automotive libraries for vehicle system modelling," in *Proc. 5th Model. Conf.* Vienna, Austria: The Modelica Association, 2006, pp. 33–41. [Online]. Available: https://www.modelica.org/events/modelica2006/Proceedings/sessions/Session1b2.pdf

[23] L. Nagel and D. Pederson, "SPICE (Simulation Program with Integrated Circuit Emphasis)," in *Proc. 16th Midwest Symp. Circuit Theory*. Waterloo, ON, Canada: University of California, 1973, p. 66. [Online]. Available: http://www.eecs.berkeley.edu/Pubs/TechRpts/1973/ERL-382.pdf

[24] L. Nagel, "SPICE2: A computer program to simulate semiconductor circuits," Ph.D. dissertation, Univ. California, Berkeley, CA, Berkeley, 1975. [Online]. Available: http://www.eecs.berkeley.edu/Pubs/TechRpts/1975/ERL-520.pdf

[25] M. ZambranoBigiarini. (2017). *hydroGOF: Goodness-of-Fit Functions for Comparison of Simulated and Observed Hydrological Time Series*. [Online]. Available: http://hzambran.github.io/hydroGOF/

[26] A. Muetze and Y. C. Tan, "Electric bicycles—A performance evaluation," *IEEE Ind. Appl. Mag.*, vol. 13, no. 4, pp. 12–21, Jul. 2007.

[27] Heinzmann GmbH. (2012). *Heinzmann Classic RN 120. Data Sheet*. Schönau, Germany, p. 2. [Online]. Available: https://www.heinzmann.com/jdownloads/electric-and-hybrid-drives/wheel-hub-motors/DS_RN-120_Wheel-hub-motor_e.pdf

[28] S. Maniktala, *Switching Power Supplies A to Z*. Burlington, MA, USA: Elsevier, 2006.

[29] S. N. Manias and S. N. Manias, "DC–DC Converters," in *Power Electronics Motivate Drive Systems*, S. N. Manias, Ed. Academic, 2017, Ch. 7, pp. 501–611. [Online]. Available: https://www.sciencedirect.com/science/article/pii/B978012811798900007X

[30] S. Jain and L. Kumar, "Fundamentals of power electronics controlled electric propulsion," in *Power Electron Handbook*, 4th ed., M. H. Rashid, Ed. London, U.K.: Butterworth, Jan. 2018, pp. 1023–1065. [Online]. Available: https://www.sciencedirect.com/science/article/pii/B9780128114070000350?via%3Dihub

[31] *RFCafe—Standard Inductor Values*. Accessed: Oct. 8, 2019. [Online]. Available: http://www.rfcafe.com/references/electrical/inductor-values.htm

[32] *Coil Winding Specialist (USA)*. Accessed: Oct. 8, 2019. [Online]. Available: http://www.coilws.com

[33] *Panasonic Corporation—Polymer Electrolytic Capacitors*. Accessed: Oct. 8, 2019. [Online]. Available: https://industrial.panasonic.com

[34] *Kemet Electronics Corporation*. Accessed: Oct. 8, 2019. [Online]. Available: http://www.kemet.com

[35] R. D. Middlebrook and S. Cuk, "A general unified approach to modelling switching-converter power stages," *Int. J. Electron.*, vol. 42, no. 6, pp. 521–550, Jun. 1977, doi: 10.1080/00207217708900678.

[36] S. M. Cuk, "Modelling, analisys and desing of switching converters," Ph.D. dissertation, California Inst. Technol., Pasadena, CA, USA, 1977. [Online]. Available: http://thesis.library.caltech.edu/1157/1/Cuk_sm_1977.pdf and http://thesis.library.caltech.edu/1157/

[37] H. Abaali, "Design modelling control and simulation of DC/DC power buck converter," *Int. J. Electr. Comput. Energ. Electron. Commun. Eng.*, vol. 9, no. 10, pp. 1229–1235, 2015. [Online]. Available: http://waset.org/publications/10003469, doi: 10.5281/zenodo.1338792.
[38] E. Fossas and G. Olivar, "Study of chaos in the buck converter," *IEEE Trans. Circuits Syst. I, Fundam. Theory Appl.*, vol. 43, no. 1, pp. 13–25, Jan. 1996.
[39] M. Otter. *Rectifiedmean*. Wessling, Germany. Accessed: Nov. 11, 2019. [Online]. Available: https://doc.modelica.org/Modelica3.2.3/Resources/helpDymola/Modelica_Blocks_Math.html#Modelica.Blocks.Math.RectifiedMean
[40] J. Blackburn, *Modern Instrumentation for Scientists and Engineers* (Springer Nature Book Archives Millennium). New York, NY, USA: Springer, 2001.
[41] T. J. Barlow, S. Latham, I. S. Mccrae, and P. G. Boulter, "A reference book of driving cycles for use in the measurement of road vehicle emissions," U.K. Dept. Transport., Berkshire, U.K., Tech. Rep. PPR354, 2009, p. 284. [Online]. Available: https://assets.publishing.service.gov.uk/government/uploads/system/uploads/attachment_data/file/4247/ppr-354.pdf

FRANCISCO J. GÓMEZ NAVARRO was born in Almería, Spain, in 1966. He received the B.S. degree in aeronautical engineering from the Universidad Politécnica de Madrid, in 1989, and the M.S. degree in computer science engineering in automatic control and industrial computing from the Universidad de Almería, Almería, Spain, in 2012. He is currently pursuing the Ph.D. degree in computer science engineering with the Centro Mixto CIESOL, Universidad de Almería.

From 1989 to 2015, he was the Design, Development and Commissioning Engineer of test equipment in the tire sector (aircraft, earth-moving, agricultural, truck, and car tire). Since 2015, he has been the manager in a tire test facility with the Centro de Experiencias Michelin de Almería. His research interests include computer vision on biomedical applications, modeling and simulation of multiphysical systems mainly in vehicle applications, and hold one patent in computer vision for biomedical applications. He is currently investigating in Electric Vehicle Energy Management.

LUIS J. YEBRA was born in Almería, Spain, in 1971. He received the Telecommunications Technical Engineer degree from the Universidad de Alcalá, Madrid, Spain, in June 1993, the Physics degree from the Universidad Nacional de Educación a Distancia (UNED), Madrid, that finalized with three prizes to the best academic curriculum, in June 1997, and the Ph.D. degree in automatic control and industrial computing from the Automatic Control and Computer Science Department, UNED, in May 2006.

From 1999 to 2007 he was a Predoctoral Fellow and a Researcher with the national research center CIEMAT, Department of Energy, Plataforma Solar de Almería (PSA-CIEMAT). Since 2007, he has been a Tenured Scientist with CIEMAT, PSA-CIEMAT center, in Dynamic Modelling and Automatic Control, mainly focused to concentrated solar thermal plants (CST). He has coauthored four books, more than 30 scientific articles published in international journals (JCR), more than 70 international conference proceeding papers, supervised three Ph.D., participated in more than 30 publicly funded research projects, two technology transfer agreements, and the creation of a spin-off company.

FRANCISCO J. GÓMEZ MEDINA was born in Almería, Spain, in 1996. He received the M.Eng. degree in mechanical engineering from the University of Bristol, Bristol, U.K., in 2018. He is currently pursuing the Ph.D. degree in manufacturing and management with the Institute for Manufacturing, University of Cambridge, Cambridge, U.K.

Throughout his undergraduate degree, he was involved in various projects at the Bristol Robotics Laboratory, such as the automated deployment and maintenance of wireless sensor networks with UAVs and perching of nanoquadcopters for data harvesting. Before starting his Ph.D., he worked as a Consultant for Scribeless, an automated handwriting start-up, where he led the first iteration of the handwriting robot. His research interests revolve around how companies can leverage digital technologies to make better decisions at various organizational levels.

ANTONIO GIMÉNEZ-FERNANDEZ was born in Almería, Spain, in 1968. He received the M.S. degree in industrial engineering from the Polytechnic University of Madrid, in 1993, and the Ph.D. degree (with extraordinary Doctorate award) in industrial engineering from the University Carlos III of Madrid, Spain, in 2000.

From 1995 to 2006, he was an Associate Professor with the University Carlos III de Madrid, and a member of the RoboticsLab research group. Since 2006, he has been an Associate Professor with the University of Almería. He has involved in more than 20 National R + D Projects (being the Main Researcher in four of them), and seven International Projects, related to Service Robotics, and processing automation (especially at the construction sector), and with machine design. Now, he belongs to Automation, Robotics and Mecatronics Group, at the Almería University. He has written 25 international JCR articles, more than 50 Conference papers, four chapters at International books. His main research fields are mechanics and electronics of assistive robot, multibody modelling applied to mechanisms and vehicle, and teleoperated systems.